FLOW FIELD IN A LIQUID IMPINGING JET CONFINED BY SLOPPING PLANE WALLS

Adélio S. Cavadas[1], João B. L. M. Campos[2] and Fernando T. Pinho [1,3]

1: Centro de Estudos de Fenómenos de Transporte, Faculdade de Engenharia da Universidade do Porto, Rua Dr. Roberto Frias s/n, 4200-465 Porto, Portugal, adelioc@fe.up.pt
2: Centro de Estudos de Fenómenos de Transporte, Departamento de Engenharia Química, Faculdade de Engenharia da Universidade do Porto, Rua Dr. Roberto Frias s/n, 4200-465 Porto, Portugal, jmc@fe.up.pt
3: Universidade do Minho, Largo do Paço, 4704-553 Braga, Portugal, fpinho@fe.up.pt

Abstract. An experimental investigation was carried out to characterize the flow field in a liquid impinging jet confined by slopping plane walls and emanating from a rectangular duct. The fluids are Newtonian flowing in the laminar (Re= 135 and 276) and turbulent regimes (Re=13,750) and the two-dimensional rectangular cell has an aspect-ratio equal to 13. The fully-developed rectangular jet impinging the flat surface (plate) is confined by two slopping plane walls, each one making an angle of 12° relative to the plate. The presence of the impact plate is felt upstream at y/H= -0.2 in the laminar regime and at y/H= -0.4 in the turbulent regime. The results show that the flow is symmetric relative to the x-y and x-z center planes. Near the plane slopping wall there is separated flow for Reynolds numbers in excess of 208, as was observed in visualization studies. For Re= 275 this small separated flow zone has a normalized length, x_R/H = 0.25, whereas for turbulent flow x_R/H is equal to 0.9. In the turbulent flow regime turbulence is very high at the jet impact region due to strong fluid deceleration, but the maximum turbulence is observed in the shear layer formed between the jet along the impinging wall and the separated flow region on the sloping wall. We also report three-dimensional effects due to finite slenderness of the flow geometry.

1. Introduction

Confined jets are frequently used to enhance heat and mass transfer since the fluid impinges the solid surface at high velocities and the boundary layer thickness is small. Confined jets are found in various industrial processes and systems such as in paper and textile drying, steel mills, tempering of glass, cooling of turbine blades and of electronic components. The objective of this work is the investigation of the flow patterns of impinging rectangular jets, confined by inclined and plane walls, for various Newtonian and non-Newtonian liquids; here, only results for Newtonian liquids in laminar and turbulent flow are presented.

Liquid single-phase impinging jets are usually either submerged or free-surface jets. In submerged jets the liquid issues into a region containing the same liquid at rest, whereas in free-surface jets the liquid jet is surrounded by ambient air or gas. Submerged jets can be unconfined or confined by a surface; in the latter case this is usually a plate attached to the nozzle and parallel to the impinging surface.

This work describes the investigation of laminar and turbulent impinging jets, confined by sloped plane walls. These extend from the exit of a rectangular duct to a short distance above the impinging plate. Previously, Garimella and Rice (1995) studied circular jets confined by a conical wall. They divided the flow field of the impinging jet into three regions: the free-jet region, the impingement region and the wall region. The flow in the free-jet region is axial and it is not affected by the presence of the impinging plate; the axial velocity starts to decay at the nozzle exit and the jet spreads to the surroundings before the impingement. Gardon and Akfirat (1965) and Martin (1977) have shown that the flow of turbulent jets starts to be affected by the impinging plate at approximately 1.2 nozzle diameters from this surface. In the present study, the duct-to-plate distance is very short, i.e. 20% of the duct height, and as will be shown, the plate effect is felt inside

the duct. At the impingement region, the fluid strongly decelerates and is forced to change its direction, flowing to the cell exits.

The emphasis in this article is the investigation of the flow hydrodynamics and the effects of several dynamic parameters. The next section describes the experimental setup and the instrumentation used, including the laser Doppler anemometer. Afterwards, the results obtained in the rectangular duct and in the cell are presented and discussed.

2. Experimental rig and instrumentation

2.1 Experimental facilities

The flow loop used in the present experiments is shown schematically in Fig. 1. Flow was provided by a progressive cavity pump [2] (mono pumps Dresser model CB081AC1A3/G, the numbers in brackets refer to components shown in Fig. 1) fed directly from a stainless steel tank of 175 l of capacity [1]. One pulsation damper [3], located immediately downstream of the mono pump outlet, was used to smooth out the flow and remove any pulsations prior to the inlet of the entrance reservoir [5]. At the top of this reservoir an air chamber dampened any residual pulsations in order to have a complete steady flow at the rectangular duct inlet. The rectangular duct [6] was made of four modules and was 2.6 m long with an internal cross section area of 0.0052 m^2 (height (H) x width (2*W) = 0.02 m x 0.26 m, corresponding to an aspect ratio (AR) of 13). Each module was constructed from stainless steel plates, machined and ground to size and then assembled with screws and a bonding agent.

The cell test section [7] is schematically represented in Fig. 2 (a), together with the coordinate system used in this work (*x* and *y* are in the paper plane and *z* is in the normal direction; the origin is at the central point of the rectangular duct exit plane), and a photo in Fig. 2(b) shows the test section. Two slopping plane walls, each one making an angle of 12° relative to the flat surface (plate), confined the jet flow inside the cell. The outgoing flow was from two channels with 4 mm height (h) and the same width as the inlet rectangular duct defining here AR=65. The reservoirs [5] and [7] and the cell were made of acrylic to allow velocity measurements using a laser Doppler anemometer (LDA).

Eleven pressure taps were drilled along the rectangular duct *x*-*y* center plane with 200 mm spacing between consecutive taps. They were used to study the development of the flow along the duct. The pressure measurements helped ensure also that the connections between the duct modules (done within machining tolerances of $\pm 10 \mu m$) did not produce any detectable perturbation to the flow .

The pressure differences between any two taps were measured by a differential pressure transducer, model P305D-S20 from Valydine. The transducer calibration was carried out in a device made up of two independent water columns with the water level checked by two precision rules with an accuracy better than 0.1 mm. All the pressure taps were drilled carefully to avoid spurious edge effects. For the design of pressure taps the recommendations of Shaw (1960) and Franklin and Wallace (1970) were followed.

An electromagnetic flowmeter, type Mag Master [4] from ABB Taylor, measured the volumetric flow rates ($\dot{Q}_{in}$) in the range of 0-5 l/s with an accuracy of 0.2% of full scale.

All the instruments were connected to a 486 PC provided with a data acquisition board interfaced with an Advantech PCLD-8115 card.

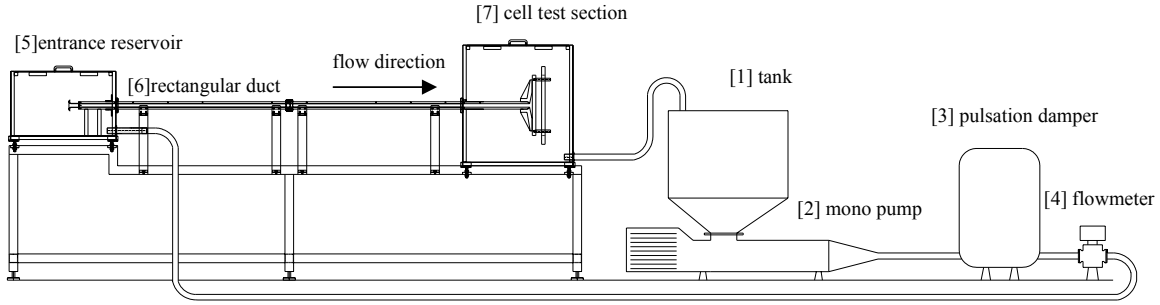

Fig. 1 Schematic of flow loop.

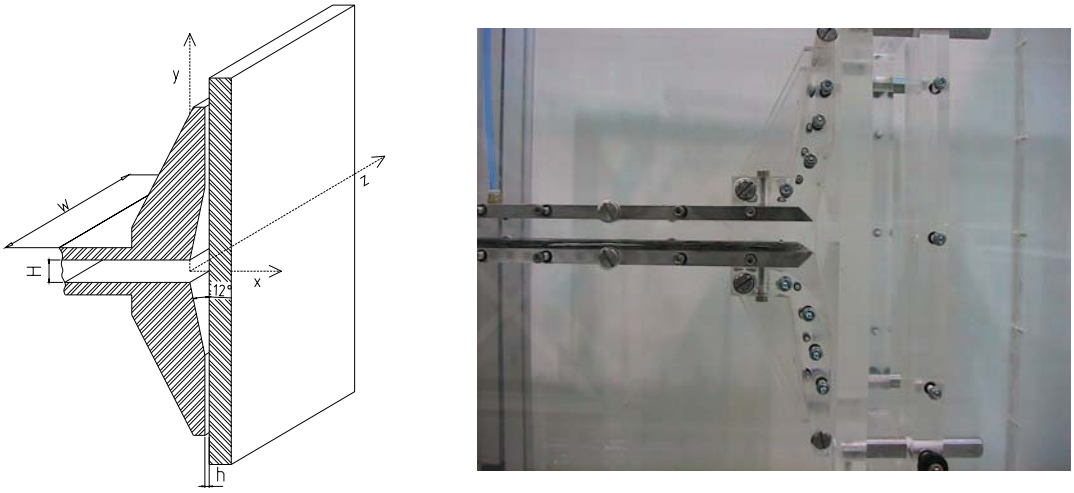

(a) (b)

Fig. 2 – Cell test section: (a) sketch of the half cell test section and coordinate system centered in the *x*-*y* and *x*-*z* plane; (b) photo of the cell test section.

2.2 Laser-Doppler system

A 1-D laser-Doppler anemometer from Dantec was used to measure the mean and fluctuating velocity fields. The LDA was used in the forward scatter mode and the light source was an air-cooled, multimode 300 mW Ar-ion laser. The beam passed through a series of optical elements before the Bragg cell, where a frequency shift of 0.6 MHz was imposed. The front lens had a 300 mm focal length. The scattered light was collected by a photo-multiplier before which stood an interference filter of 514.5 nm. After being band-pass filtered, the signal from the photo-multiplier was processed by a TSI 1990C counter operating in the single measurement per burst mode with a frequency validation setting of 1% in the 10/16 cycle comparison. A 1400 Dostek card interfaced the counter with an 80486 based computer to provide all the statistical quantities via a purpose-built software. For each point measured, a sample size of 10000 values was taken. The refraction of the laser beams at the plane walls of the duct and of the cell was taken into account to correct the position of the control volume. Table 1 provides the main characteristics of the LDA.

Laser wavelength	514.5 nm
Measured half angle of beams in air	3.65°
Dimensions of the measuring volume in air	
major axis	2.53 mm
minor axis	146 μm
Fringe spacing	4.041 μm
Frequency shift	0.6 MHz

Table 1 - Main characteristics of the LDA in air at e^{-2} intensity.

The LDA probe was mounted on a milling table with movement in the three spatial coordinates. The system was used to measure both the mean and fluctuating velocities in the horizontal (u and u`) and vertical ($v$ and $v$`) directions along the duct and inside the cell. For the horizontal velocity component inside the rectangular duct the laser beams were set to cross each other in a horizontal plane and measurements could be performed well into the viscous sublayer..

Near the sloped wall, inside the cell, the horizontal velocity component could not be measured directly because one of the beams collided with the wall. In such cases the u velocity component was determined using trigonometry and measurements of the vertical velocity component and of a velocity component at an angle of 24º with the vertical direction. Because of optical access, these velocity measurements inside the cell were not performed at the centre-plane, but at a plane (z/W = 0.45) closer to the side wall, where the end wall did not affect the flow, as will be shown in Section 4. Typical uncertainties associated to the mean and fluctuating streamwise velocity data were estimated to be 1 % and 4 %, respectively. This increased to 2% and 5% for transverse mean and fluctuating velocities and to 3.5% and 14% for the indirectly measured mean and fluctuating horizontal velocities inside the cell, respectively.

3. Fluids

The fluids used were tap water, and an aqueous glycerol solution for the turbulent and laminar flow measurements respectively. At 20ºC the density and dynamic viscosities of these fluids were : 1000 kg/m3 and 0.001 Pa.s for water; 1184 kg/m^3 and 0.0425 Pa.s for the glycerin solution. The shear viscosities were measured with a rheometer from Physica, model Rheolab MC 100, using the low viscosity double-gap concentric cylinder system. This geometry allowed the measurement of viscosities between 1 mPa.s and 67.4 mPa.s, at a maximum shear rate of 4031 s-1. A thermostatic bath and a temperature control system, Viscotherm VT, allowed the control of the temperature of the fluid sample within 0.1º C. The fluid densities were measured with a picnometer.

4. Experimental results

4.1 Fully-developed flow in the rectangular duct

Transverse profiles of streamwise velocity were measured along the rectangular duct and compared with theoretical expressions for fully-developed flow. In the laminar regime the Reynolds numbers were 136 and 275 and in the turbulent regime it was 13,750. The Reynolds number is based on the mean inlet velocity,U , measured with the flowmeter, while the length scale is the

hydraulic diameter of the rectangular channel. The mean velocity data are normalized with the mean velocity at the rectangular channel, the x and y coordinates are made non-dimensional by the height of the duct (H) and the z coordinate by the half-width of the channel (W).

In Fig. 3(a) the measured profiles at both laminar Reynolds numbers, in the fully developed region (x/H= -5.7) are compared with the theoretical expressions for the rectangular duct flow (AR=13) presented in White (1991) and the parallel plate flow (AR=∞). The measured data lies between the two theoretical curves which differ only by 2%.

The symmetry relative to the x-y centre-plane was measured and the corresponding spanwise profiles of streamwise velocity at x/H= -5.7 are shown in Fig. 3 (b) for Re=136 and Re=13,750. The filled symbols represent, for each case, the reflected profile from one half of the duct into the other half. For both Reynolds numbers the flow is symmetric and the presence of the end walls is not felt in the bulk of the flow, between z/W =$\pm$ 0.7 in the laminar regime and z/W = $\pm$ 0.6 in the turbulent regime.

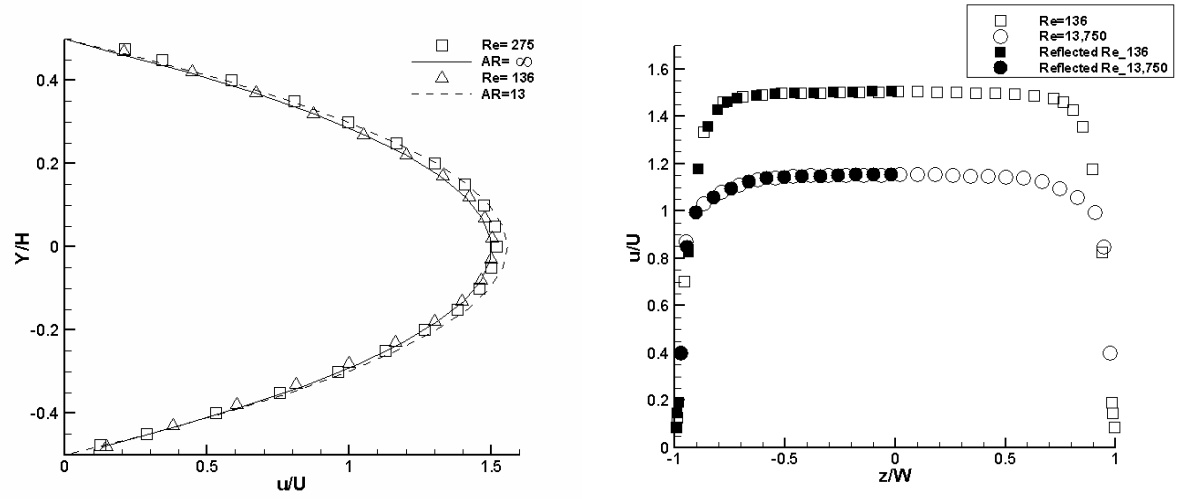

(a) (b)

Fig. 3 – (a) Comparison between measurements (symbols) and theoretical expressions (lines) at x/H= -5.7. (b) Spanwise profiles of streamwise velocity at y/H =0, x/H= -5.7 for Re=136 and Re=13,750

For turbulent flow, the measured velocity profile is compared in Fig. 4 (a) with Spalding's law in wall coordinates (c.f. White, 1991). The comparison is excellent and velocity data could be measured inside the viscous sublayer, down to about $y^+\approx$ 1. The streamwise rms velocities, normalised by the friction velocity, compare well with DNS data from Kim et al (1987) for plane channel flow in Fig 4(b). The streamwise intensity u' scales with the inner variables starting from the wall up to the point of maximum intensity (u'^+= 2.55) located at $y^+ \approx 15$. The friction velocity was obtained independently from pressure drop measurements. These measurements resulted in friction factors of 0.68, and 0.030 at Reynolds numbers of 136 and 13,750 respectively in agreement with the theoretical value of 0.647 given by White (1991) for laminar flow at Re= 136 and of 0.031 given by Dean (1978) for turbulent flow at Re= 13,750. Based on the velocity and pressure measurements it was concluded that the flow was able to become fully developed upstream of the cell for the investigated laminar and turbulent flows.

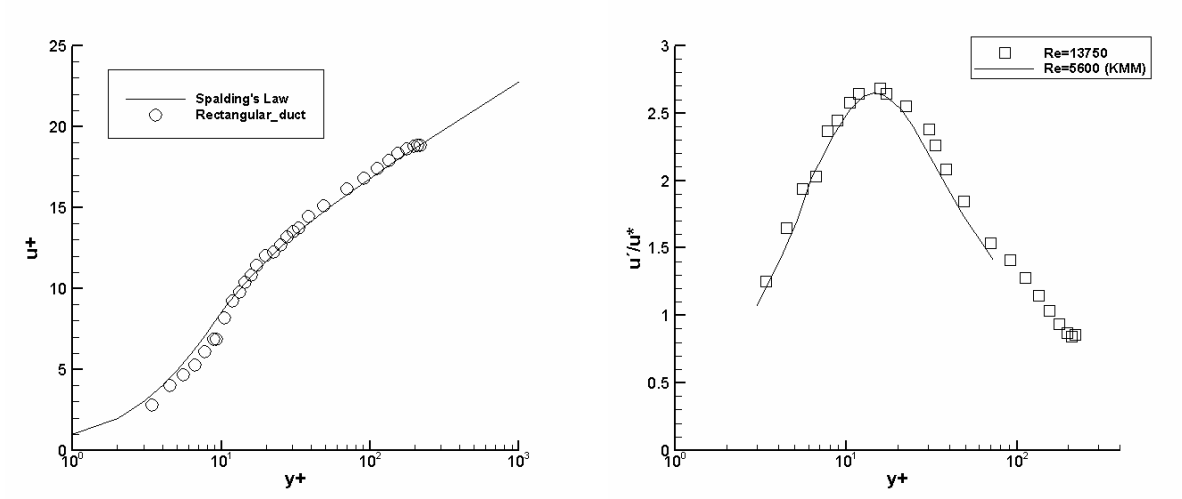

(a) (b)

Fig. 4 - Comparison between experimental data (symbols) and theoretical results (lines) in wall coordinates at x/H= -5.7 and Re= 13,750: (a) Streamwise mean velocity profile; (b) Streamwise rms velocity profile.

4.2 Flow pattern within the cell an in the approach flow

4.2.1 Laminar regime

The progression of the streamwise velocity at the end of the rectangular duct and in the impinging jet region is shown in Fig 5(a) along the x-y centre-plane. The first profile, at x/H=-5.7 corresponds to the fully-developed flow. At x/H=-0.4 the effect of the plate is still rather weak, with values of velocity differing from the fully-developed profile by less than 2.5 %. The decrease of velocity near the centreline and flow acceleration near the walls is clear as the fluid approaches the plate, especially after the fluid exits the rectangular duct when a large drop in u-velocity is seen and the no-slip condition ceases to apply because the upper and lower walls end. Fig 5(a) also shows symmetry relative to x-z centre-plane.

These features are also seen in the vector plot of Fig. 5(b) for Re= 136. The flow turns into the cell with most of the fluid flowing along the impinging plate. In spite of the strong turn, the vector plot and measurements of velocity along the slopping wall did not show any separation (these were measurements of the velocity component parallel to the sloping wall taken along the wall at a distance of 150 μm). This is probably due to the very favourable pressure gradient imposed by the conical shape of the cell.

Inside the cell the flow separates symmetrically and this is well seen in the vector plot of Fig. 6 which shows the upper half of the whole cell and the lower half of the impact region and end of the rectangular duct geometry for Re=136. At the end of the cell the vector plots show a parabolic-like shape suggesting that the flow becomes again fully-developed. Note that at the exit the flow is now characterized by a Re= 68.

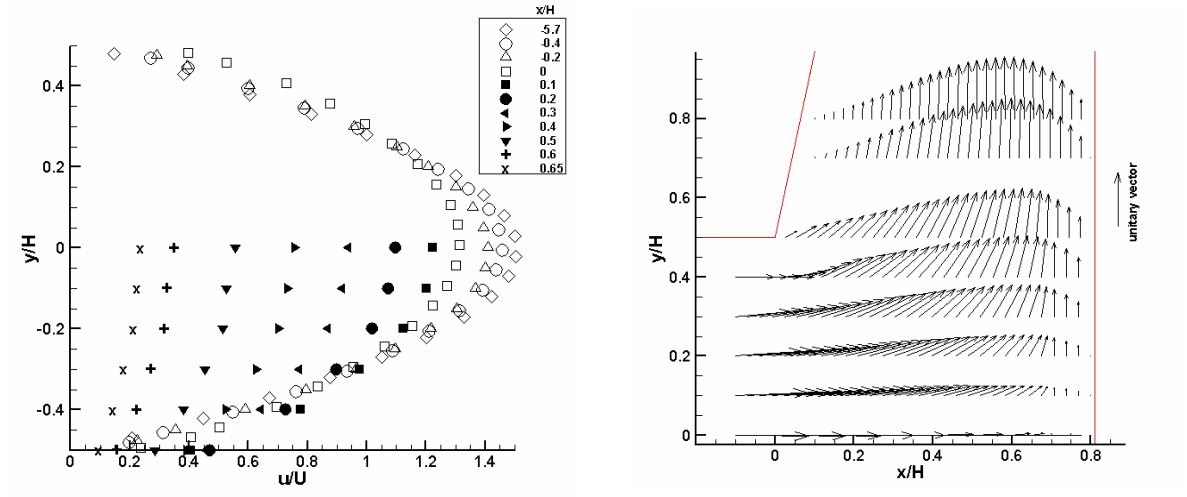

(a) (b)

Fig. 5 - Flow at the end of the duct and in the impact region for *Re*= 136: (a) Transverse profiles of streamwise velocity at =0. (b) Vector plot at =0.45.

The flow symmetry inside the cell is shown in Fig. 7. The profiles of the streamwise velocity in the cell (*v* component) in Fig. 7(a) at Re=136 indicate symmetry in the spanwise direction where the closed symbols are the reflection of the velocity profile on one side of the duct onto the other half. In Fig. 7(b) we show transverse profiles of the streamwise velocity inside the 4mm (*h*) wide channel and the profiles at two symmetric stations (*x/h*= ±4.9) are compared (the velocities at *x/H*= -4.9 are negative and hence were multiplied by -1). The differences between the two velocity profiles do not exceed 4%, which is a very small value considering the uncertainty in setting up the width of the two channels to within ± 0.2 mm. The figure also includes the theoretical profile for fully-developed laminar in a rectangular duct at *Re*= 68 and AR=65, and its comparison with the measured profiles provides an idea of how far the flow at the cell exit is from a fully-developed condition. Note that these profiles are here normalised by the inlet duct bulk velocity rather than by the local bulk velocity.

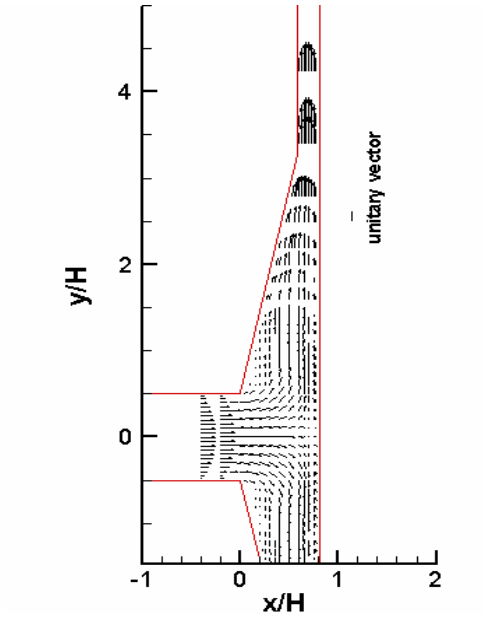

Fig. 6 – Vector plot of u and v mean velocity components at *z/W*=0.45 for Re= 136.

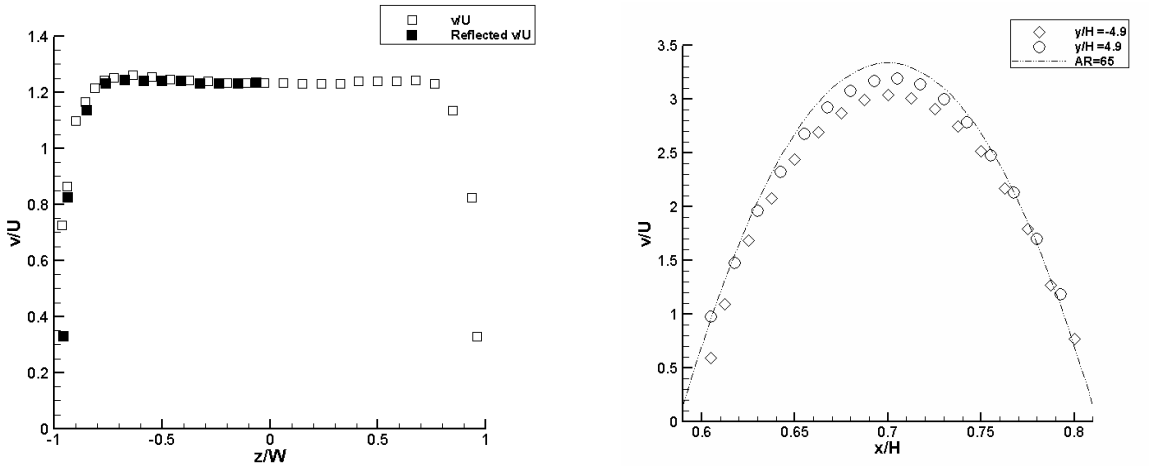

(a) (b)

Fig. 7 - Profiles of streamwise velocity in the cell for *Re*= 136: (a) Spanwise profiles at *y*/*H*=1.65, *x*/*H*=0.525.(b) Transverse profiles at *y*/*H*=4.9 and -4.9 in the plane z/W=0.45.

Flow visualizations that were carried out in the laminar flow regime have shown that although at 136 there was no flow separation within the cell, there was a visible recirculation in the centre-plane for Re > 208. Its existence is seen in the streamline plot of Fig. 8(a) for *Re*=275. The length of this centre-plane recirculation zone, measured along the inclined wall, is x_R/H =0.25.

In Fig. 8(b) profiles of the vertical velocity component inside the cell are shown for both laminar Reynolds numbers. For Re= 275 the velocities near the slopping wall are lower than those for Re=136 in agreement with the finding of a separated flow region. Then, in the central region of the cell the velocities are similar for both Reynolds numbers and near the vertical wall they become higher for *Re*= 275 to compensate for the lower flow rate near the sloping wall. These findings have also been confirmed by numerical simulations, but these are to be presented in a forthcoming paper.

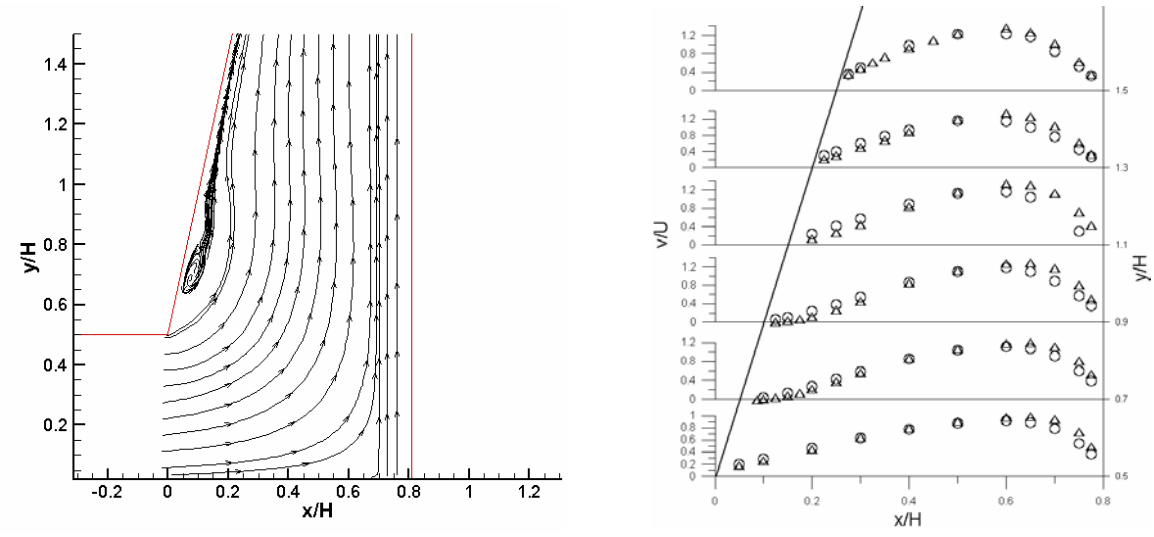

(a) (b)

Fig. 8 - Flow within the cell for *Re*= 275 and comparison with *Re*= 136. (a) Streamlines at *z*/W=0.45. (b) Vertical velocity profiles at *z*/*W*=0.45: O Re=136 and Δ Re=275.

4.2 Turbulent regime

For the turbulent flow case, Re=13,750, the influence of the impinging plate on the approach flow is shown in Fig.9 both in terms of mean and fluctuating velocities. We see a progressively lower streamwise velocity in the center of the duct as the fluid approaches the plate (see Fig 9a) and an increase of the velocity and its gradient near the wall. As the rectangular duct ends the profiles become nearly plug-like in contrast to the laminar flow case. The influence of the flow impact is also felt earlier than for the laminar case, at x/H=-0.4, which is quite surprising.

The corresponding turbulence profiles in Fig 9(b) also show these effects. Inside the rectangular duct, the large increase in streamwise velocity, and in particular its gradient, increases turbulence production by shear near the wall and large rms peaks develop there, whereas in the centre of the duct the turbulence remains largely unaffected. The strong flow deceleration after the end of the inlet duct, however, leads to large turbulence production by normal strain-normal stress interaction at the center of the duct and this is seen here as a large increase in rms. Downstream of the inlet walls, the turbulence decreased because the intense shear production disappeared and the highly turbulent flow has been advected towards the cell by the increasing vertical velocities.

As for laminar flow, the turbulent flow remains symmetric relative to both centre-planes and this is seen in Fig 10. Fig 10(a) shows the symmetry along the spanwise direction inside the cell, whereas in Fig 10(b) we compare the exit velocities in the upper and lower exit rectangular channels. The differences in mean velocity are smaller than observed for the laminar flow (c.f. Fig 7(b)). Figure 10 also shows the symmetry in terms of the rms profiles. The comparison of the rms profiles in Fig 10b) is less favourable than for the mean. For both the mean and rms velocities, the assumption that at =0.45 the flow is not affected by the presence of the end walls remains valid.

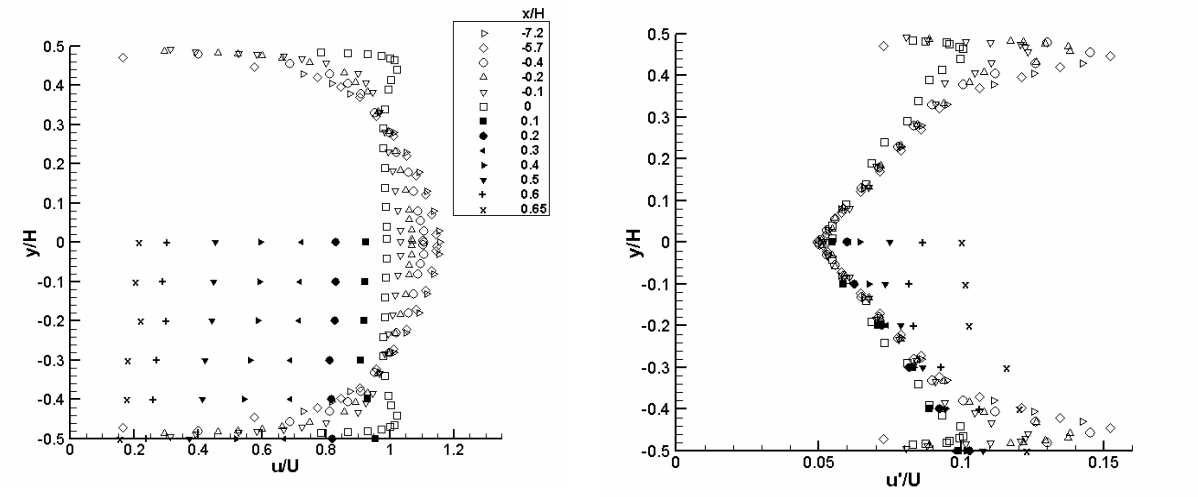

(a) (b)

Fig. 9 - Transverse profiles of streamwise velocity at the end of the duct and in the impact region for *Re*= 13,750 and *z*/W=0.45: (a) Mean velocity. (b) Fluctuating velocity.

Figure 11 shows vector plots and streamlines of the flow inside the cell. In contrast to the low Reynolds number laminar flow cases studied, there is a strong and large separated flow region with a normalised length x_R/H =0.9 quantified from measurements of velocity along the inclined wall. The flow inside the cell is seen to accelerate along the flat wall, first because of the presence of the separated flow region and afterwards because of the narrowing of the channel due to the slopping wall. Transverse profiles of the vertical velocity inside this cell are shown in Fig 12 (a), with the

corresponding profiles of the normalized rms of the fluctuating vertical velocity plotted in Figure 12 (b).

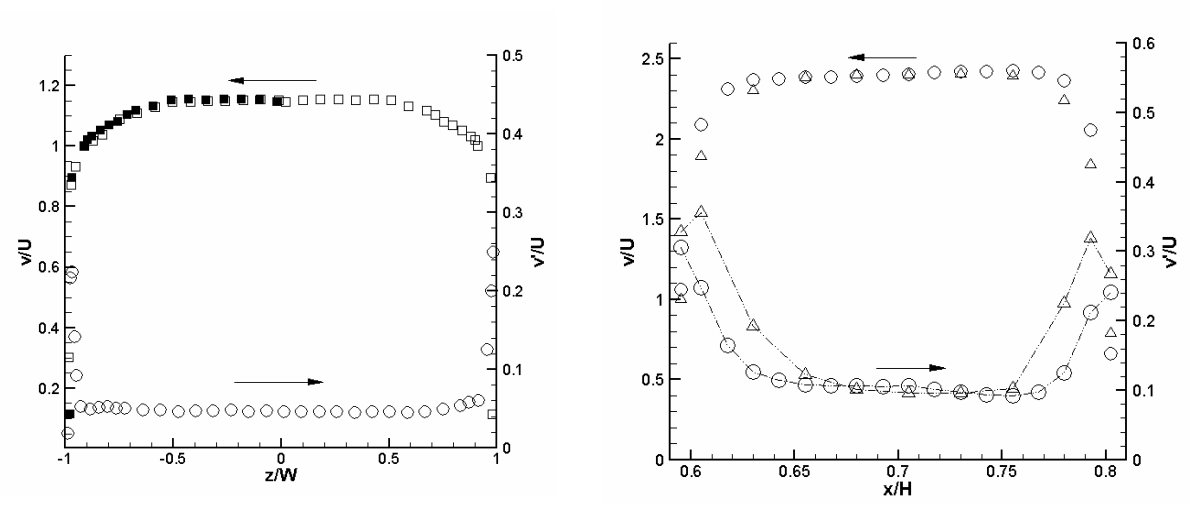

Fig. 10 - Profiles of streamwise velocity inside the cell for *Re*= 13,750: (a) Spanwise profiles at *y*/*H*=0.6, *x*/*H*=0.45,. (b) Transverse profiles at : O *y*/*H*=4.25 and Δ *y*/*H*= -4.25.

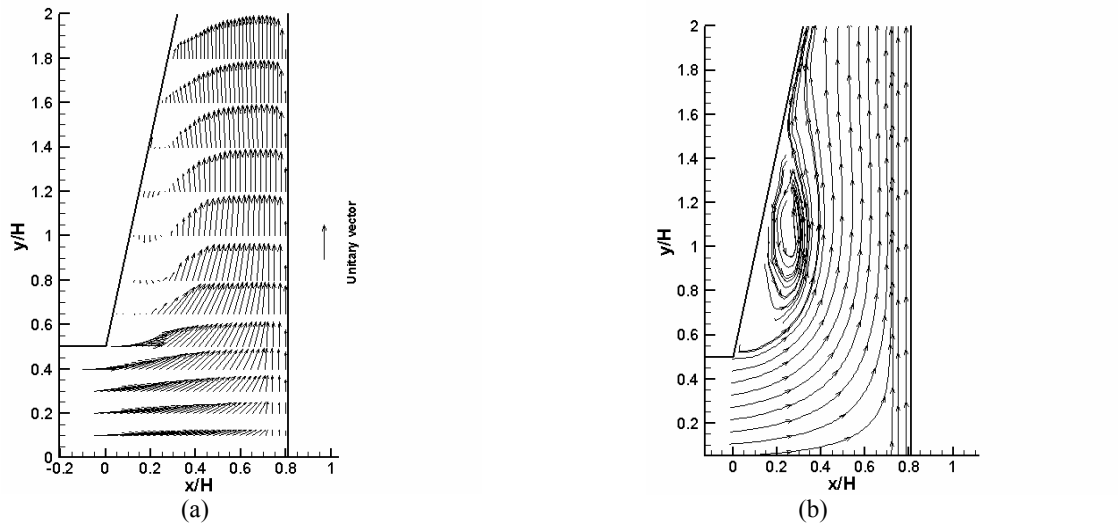

Fig. 11 - Flow characteristics inside the cell for *Re*= 13,750: (a) Vector plot at *z*/*W*=0.45. (b) Streamlines based on *u* and *v* velocity components.

A region of high *u*' turbulence was observed in the impinging region, near the place where the rectangular jet hits the plate, due to the strong flow deceleration (c.f. Fig. 9(b)). However, this is not the region of maximum turbulence, which is found inside the cell. The profiles in Fig. 12(b) show here the existence of two regions of peak turbulence where its production is by the shear rate- shear stress mechanism: one region is along the boundary layer at the vertical plate whereas the second region, where turbulence is maximum, is in the shear layer between the separated flow region and the central jet. This has also been confirmed by contours drawn for the whole geometry, not shown here for space limitations. Downstream of the separated flow region, the turbulence keeps increasing near the flat wall because of the larger shear rates associated with flow acceleration to

conserve mass, even though the flow acceleration acts as a sink of turbulence. This indicates that the production of turbulence by shear at the wall overcomes the reduction of turbulence due to flow acceleration.

The complexity of this flow, the imbalance of normal Reynolds stresses that it creates and the effect of the flat walls on the sides, leads to a characteristic three-dimensional effect near these flat walls, which eliminates the separated flow regions there. This three dimensional flow feature was visualized and will be shown and discussed in the next section.

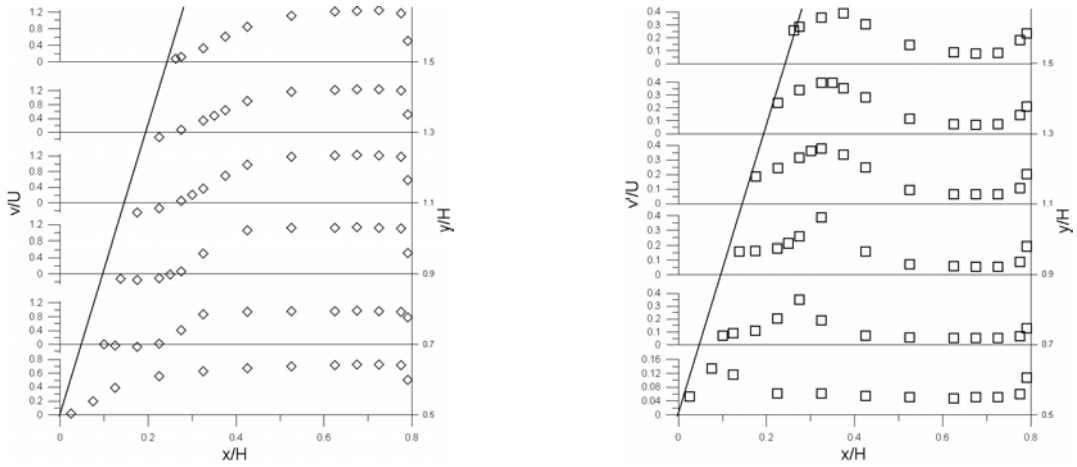

(a) (b)

Fig. 12 –Transverse profiles of mean (a) and fluctuating (b) vertical velocity inside the cell at *z/W*=0.45, for Re=13,750.

4.3 Three dimensional effect

Some spanwise profiles of the vertical velocity measured inside the cell are plotted in Fig. 13 (a). These show that local maxima and minima in the vertical velocity are stronger near the slopping wall and at the beginning of the narrowing cell. Simultaneously, no separated flow regions zones were seen near the flat side walls. Visualizations of the flow using a die injection technique, but especially small tracer bubbles and a video camera, have shown a helical flow motion depicted schematically in Fig. 13 (b). Before reaching the end walls, the fluid (bubbles) in the helical motion exits the separated flow region, which vanishes, and merges into the main flow creating a vertical wall jet. The wall jets are the peaks of vertical velocities seen near the end walls (at $z/W \approx -0.9$ for $y/H = -1.75$, $x/H = 0.525$ and $x/H = 0.3$), just downstream the separated flow. Further downstream along the converging channel the jet weakens and the velocities rise due to continuity. Still, there are traces of a perturbation in the velocity profiles ($z/W \approx -0.95$ for $y/H = -3.1$, $x/H = 0.575$ and $x/H = 0.675$).

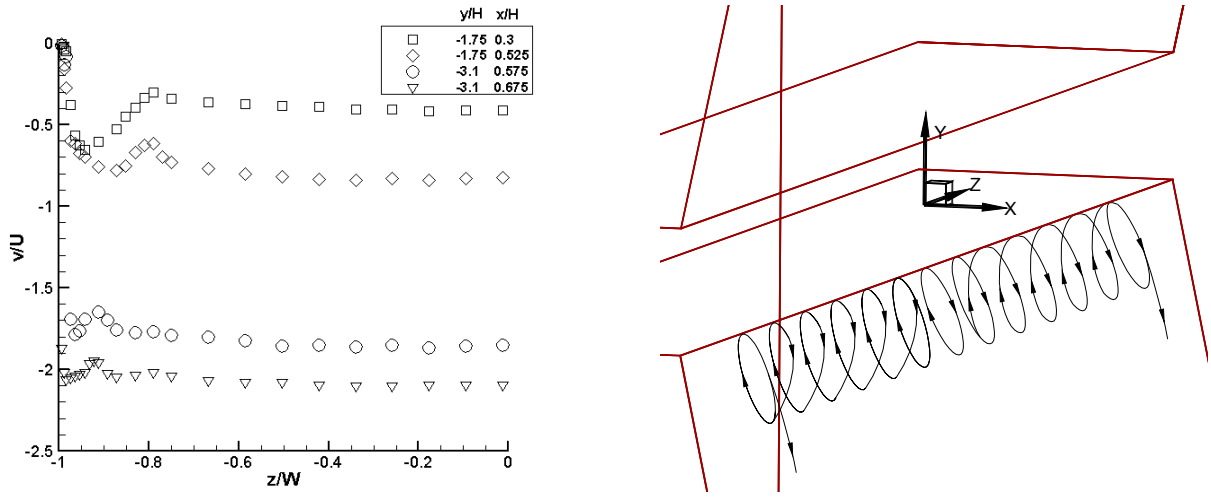

(a) (b)

Fig. 13 - Three dimensional flow effect near the side walls for *Re*= 13,750(a) Spanwise profiles of streamwise velocity at various locations. (b) Sketch of the there-dimensional flow in the separated flow region.

4. Conclusions

The flow field created by liquid impinging jets in a cell confined by a slopping plane wall has been studied for Newtonian fluids in the laminar and turbulent regimes using pressure variations and laser-Doppler anemometry. The flow field in the approach rectangular duct was fully-developed and the flow in the center of the duct was not influenced by the presence of the end walls due to the large aspect ratio used (AR=13). The flow was everywhere symmetric relative to the *x*-*y* and *x*-*z* centre-planes. In the laminar flow a recirculation zone developed in the *x*-*y* centre-plane for Reynolds numbers in excess of 208, and for a Reynolds number of 275 the normalized length, x_R/H, was equal to 0.25 whereas for turbulent flow it is equal to 0.9 suggesting a much strong recirculating flow in latter regime. A three dimensional effect, characterized by a wall jet near the side walls, the absence of a separated flow region near the side walls and a symmetric helical motion of the separated fluid from the *x*-*y* centre-plane towards the side walls, was visualized and some of its characteristics measured by LDA.

5. Acknowledgements

The authors acknowledge funding by FCT and FEDER via the budget of Centro de Estudos de Fenómenos de Transporte and project POCI56342/EQU/2004 and A. S. Cavadas is grateful to FCT for the PhD grant BD/7091/2001.

6. References

Dean, R.B.,"Reynolds number dependence of skin friction and other bulk flow variables in two-dimensional rectangular duct flow", *J. Fluids Eng.*, 100, 215 (1978).

Franklin, R.E., Wallace, J.M., "Absolute measurements of static-holeerror using flush transducers", *J. Fluid Mech*., 42, 33-48.

Gardon, R. and J. C. Akfirat, "The role of turbulence in determining the heat transfer characteristics of impinging jets", *International Journal of Heat and Mass Transfer*, 8, 1261- 1272 (1965).

Garimella, S. V., and R. A. Rice, "Confined and submerged liquid jet impingement Heat transfer", *ASME J. Heat Transfer*, 117, 871 (1995).

Martin, H., "Heat and Mass transfer between impinging gas jets and solid surfaces", *Adv Heat Transfer*, 13, 1 (1977)

Kim, J., Moin, P., Moser, R., "Turbulence statistics in fully developed channel flow at low Reynolds numbers", *J. Fluid Mech.* 177, 133-166 (1987).

Shaw, R., "The influence of hole dimensions on static pressure measurements", *J. Fluid Mech*., 7, 550-564 ((1960)

White, F. M., "Viscous Fluid Flow",2nd ed. *McGraw-Hill*, (1991).